Nanoscale

Accepted Manuscript

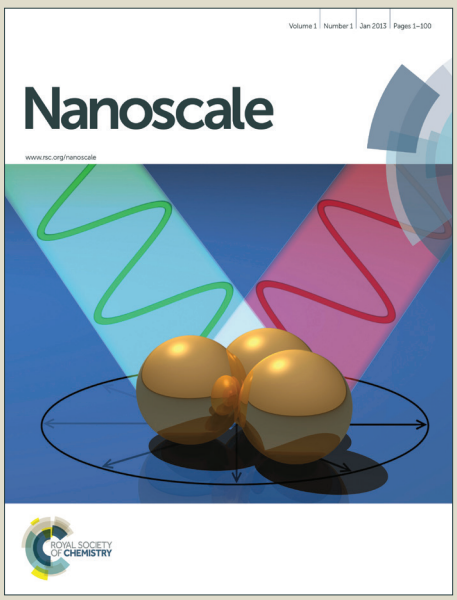

ROYAL SOCIETY OF CHEMISTRY

www.rsc.org/nanoscale

Nanoscale

RSCPublishing

PAPER

Enhanced capacitance of composite TiO_2 nanotube / boron-doped diamond electrodes studied by impedance spectroscopy

Cite this: DOI: 10.1039/x0xx00000x

Received ooth January 2012,
Accepted ooth January 2012

DOI: 10.1039/x0xx00000x

www.rsc.org/

K. Siuzdak[a], R. Bogdanowicz[b*], M. Sawczak[a] and M. Sobaszek[b]

We report on the novel composite nanostructures based on boron-doped diamond thin film grown on top of TiO_2 nanotubes. The nanostructures made of BDD-modified titania nanotubes showed an increase in activity and performance when used as electrodes in electrochemical environments. The BDD thin films (~200-500 nm) were deposited using microwave plasma assisted chemical vapor deposition (MW PA CVD) onto anodically fabricated TiO2 nanotube arrays. The influence of boron-doping level, methane admixture and growth time on the performance of Ti/TiO2/BDD electrode was studied in detail. Scanning electron microscopy (SEM) was applied to investigate the surface morphology and grain size distribution. Moreover, the chemical composition of TiO_2/BDD electrodes was investigated by means of micro-Raman Spectroscopy. The composite electrodes TiO_2/BDD are characterized by the significantly higher capacitive current comparing to BDD film deposited directly onto Ti substrate. The novel composite electrode of TiO2 nanotube array overgrown by boron-doped diamond (BDD) immersed in 0.1 M $NaNO_3$ can deliver specific capacitance of 2.10, 4.79, 7.46 mF cm^{-2} at a scan rate of 10 mV/s for [B]/[C] ratio 2k, 5k and 10k, respectively. The substantial improvement of electrochemical performance and excellent rate capability could be attributed to synergistic effect of TiO_2 treatment in CH_4:H_2 plasma and high electrical conductivity of BDD layer. Analysis of electrochemical impedance spectra according to electric equivalent circuit allows to determine surface area on the basis of value of constant phase element.

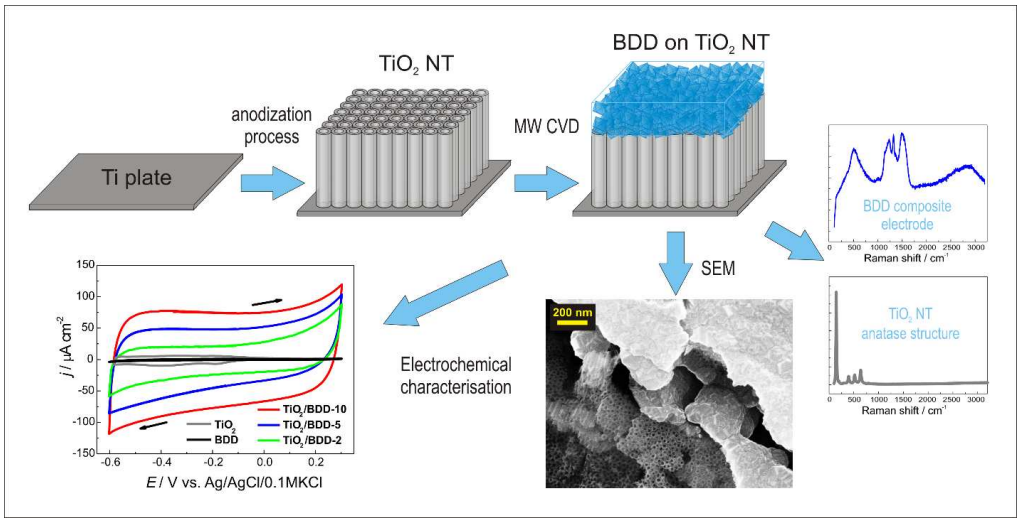

Nanoscale RSCPublishing

PAPER

Introduction

Recently, the emerging need for efficient energy storage devices has motivated researchers to discover, develop, and assemble new classes of nanomaterials. Supercapacitors, among others, attracted growing scientific interest in last decade.[1,2] Two supercapacitor types should be mentioned, i.e. electrical double layer capacitors[3] and pseudocapacitors that are powered by Faradaic reactions carried out on the electrode material.[4] The most critical approaches with regard to the enhancement of electrochemical capacitance are the development of nanostructured electrodes with a large effective area, and an increase in the electrical conductivity of electrodes by using highly conductive materials. [5]

The anodic titanium dioxide nanotube arrays provide a large specific surface area as well as a direct pathway for charge transport, thus holding promising capabilities applicable to supercapacitors.[6] Nevertheless, the capacitances based on TiO_2 nanotubes (without intentional doping) are generally limited to less than 1 mF cm^{-2}, mainly due to the poor electrical conductivity.[5] The reported maximum capacitance of rutile film is 40 nF cm^{-2}, which might be considered negligible.[7] On the other hand, Zhou *et al*. reported on self-doping resulting in donor states (Ti^{3+}) in TiO_2 lattice[8], which provides capacitance of 1.84 mF cm^{-2} at a scan rate of 5 mV s^{-1}, that is almost 40 times higher in comparison to pristine titania nanotube. Moreover, Lu and Li *et al.* demonstrated that hydrogenated TiO_2 (H-TiO_2) nanotube arrays display improved performance as electrode material for supercapacitors.[9,10] H-TiO_2 nanotubes were fabricated by heating TiO_2 nanotubes to the temperature between 300 and 600 °C under hydrogen atmosphere, which resulted in the specific black colour of the surface; at 400 °C the capacitance reached 3.24 mF cm^{-2}. Wang and Leshuk *et al.* produced the same black H-TiO_2 under hydrogen plasma featuring a crystalline core/amorphous shell structure and a strong absorption in the visible- and infrared-light region.[11,12] The large absorption was attributed to the localized surface plasmon resonance from the high carrier concentration in the hydrogenated shell.

Another approach concerning the increase of electrical conductivity of electrode was application of carbon materials that are regarded as excellent electrical conductors. They are often used in form of composites with metal oxide electrodes.[13,14] Moreover, various carbon forms like nanotubes[15], nanowires[16,17] or nanosheets[18] have been studied. However, these forms are often mechanically and chemically unstable[19] or not resistant to high power/ temperature.[20]

Since diamond has many excellent physical and chemical characteristics, it has variety of applications to electronic devices and diamond semiconductors [21,22]. Diamond can be n- and p-type doped to switch its properties from insulating to semiconducting and metallic, thereby changing its appearance from transparent (optical gap of 5.47 eV) to black.[23]

The p-type boron-doped diamond (BDD) shows the outstanding electrochemical properties, including wide potential window, low background current, and extreme stability, together with its inherent biocompatibility and chemical inertness, which makes the conductive BDD thin films an interesting candidate for supercapacitor electrode.[24–26]

Currently, there is tremendous interest in fabricating diamond nanostructures due to their extraordinary mechanical, electrical, and optical properties as theoretically predicted for quasi one-dimensional sp^3 nanostructures.[27,28] The investigated three-dimensional diamond includes nanowires, nanorods[29–31], teepee-shaped[32], various carbon nanowalls[33–35], porous[36] and nanostructured honeycomb[37] structures. Whereas synthesizing or fabricating these 3D composite nanostructures experimentally need several technological steps (e.g. surface pre-treatment, thin film growth and plasma etching).

Thus, we proposed fabrication of electrode material dedicated to supercapacitor that is based on anodically fabricated TiO_2 nanotubes array and the highly conductive boron-doped diamond film. Moreover, the titania nanotubes could be used as a special fracture surface for synthesising composite diamond nanostructure.

Such an approach to titania nanotubes modification by BDD thin film for electrochemical applications has not been reported until now. Therefore, the objective of the present paper is to investigate a novel composite electrode of TiO_2 nanotube array overgrown by boron-doped diamond (BDD) in MW PA CVD process. It is worth noting that the hydrogen rich plasma with methane admixture is used for BDD deposition introducing a synergistic effect of capacitance increase. First the CH_4:H_2 plasma treatment and second high electrical conductivity of BDD layer are main parameters influencing electrochemical performance of TiO_2/BDD. Thus, the fabricated TiO_2/BDD heterostructures are result of two competing processes existing at the same time: BDD layer growth and hydrogen rich plasma surface treatment. The advanced surface analysis and electrochemical characterization were conducted to investigate the surface morphology, chemical composition, electrical conductivity, and electrochemical properties of the fabricated composite BDD/titania nanotube electrodes.

Experimental

Titania nanotube arrays were formed by anodization of 0.5 mm thick titanium plates (1 x 1 cm, ASTM Grade 1, 99.5%, Spinex, Poland). Before nanotube formation, titanium foil was ultrasonically cleaned in acetone, ethanol and water. Anodization took place in two-electrode cell where Pt gauze served as a cathode and titanium substrate as anode. Electrodes were immersed in ethylene glycol solution containing 2% v/v of water and 0.3% wt NH_4F. Samples were anodized at electrode potential established at 60 V for 1 hour at 20 °C and under continuous electrolyte stirring. After anodization,

samples were immersed in deionized water and dried on the hotplate at 80 °C. Finally titania nanotube samples were annealed at 450 °C for 1 h using heating rate of 2 °C/min. in a tube furnace in oxygen atmosphere (in order to remove organic residues from electrolyte) and allowed to cool gradually back to the ambient conditions.

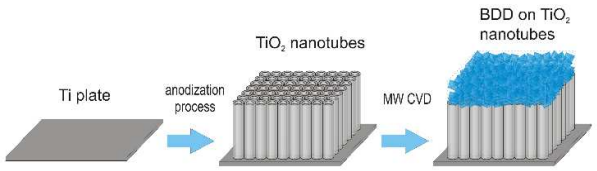

Fig. 1 Formation scheme of composite TiO_2 nanotube / boron-doped diamond electrode.

The boron-doped diamond were synthesized in an MW PA CVD system (SEKI Technotron AX5400S, Japan) on titanium and titanium/titania nanotubes substrates (see Fig. 1). Substrates were seeded using seeding media of diamond suspension (DMSO/DND- 0.5% w/w) stabilized by polyvinyl alcohol (PVA) by means of spin-coating. Substrates were spin three times with 3000 rpm. During the deposition process substrates was kept at 500 °C. In temperature range above 500°C titania nanotubes change their crystalline phase from anatase to rutile one.[38] Excited plasma was ignited by microwave radiation (2.45 GHz).[39,40] The plasma microwave power, optimized for diamond synthesis, was kept at 1300 W. The molar ratio of CH_4-H_2 mixture was kept in this study at 4 % of gas volume at 200 sccm of total flow rate. The methane admixture (4%) provides higher growth rate of diamond avoiding long treatment of partially encapsulated TiO_2 surface by hydrogen rich plasma. Moreover, BDD films result in smaller diamond crystals size and lower stress showing better adhesion and contact to titania nanotubes.[41] The base pressure was about 10^{-6} Torr and the process pressure was kept at 50 Torr. The boron level expressed as [B]/[C] ratio in the gas phase was 2000, 5000 or 10 000 ppm. The diborane (B_2H_6) was used as dopant precursor. The growth time was 1 h, producing microcrystalline film of ca. 400 nm thickness. According to the [B]/[C] ratio, prepared samples were ascribed as TiO_2/BDD-2k, TiO_2/BDD-5k and TiO_2/BDD-10k.

The molecular structure of electrode surface was analysed using Raman technique. The Raman spectra were recorded at room temperature using micro-Raman system (InVia, Renishaw, UK) and 514 nm argon ion laser as excitation. Spectra were recorded in the range of 120 – 3300 cm^{-1}.

The surface morphology was analyzed with Scanning Electron Microscope (SEM) (EVO-40, Zeiss, Germany).

The electrochemical measurements of composite electrodes were performed by the potentionstat-galvanostat system AutoLab PGStat 302N in a standard three-electrode assembly at 295 K. Different types of Ti/TiO_2/BDD working electrodes were assessed, while the Ti/BDD electrode was investigated for comparative purposes. The counter electrode consisted of Pt gauze and Ag/AgCl/0.1 M KCl reference electrode. The electrodes with geometrical surface area of 1 cm^2 were tested by cyclic voltammetry in solutions of 0.1 M $NaNO_3$ without and with 1 mM $K_3Fe(CN)_6$. Prior to taking electrochemical measurements, the electrode was pre-treated by holding it at -0.1 V for 60 s in 0.5 M HNO_3. According to Oliveira *et al.*,[42] cathodic pre-treatment, in opposite to anodic one, leads to reversible response of BDD electrode in the presence of hexacyanoferrate (II)/(III) redox couple without changing original BDD surface physical and chemical properties.[43] It should be noted, that after cyclic voltammetry measurements covering 100 cycles any mechanical and electrochemical degradation was not observed. The electrochemical impedance spectroscopy (*EIS*) measurements were carried out at ferii/feroocyanide formal redox potential in the frequency range from 0.1 to 1000 Hz and amplitude of 10 mV rms. All electrolytes were purged with argon for 50 min. before electrochemical testing, while an Ar-cushion was present above the electrolyte during the measurements.

The impedance data were analyzed on the basis of an electric equivalent circuit *(EEQC)* by using an *EIS* Spectrum Analyser[44]. The modified Powell algorithm[45] was used with amplitude weighting r_a:

$$r_a(\omega, P_1 \ldots P_M) = r_c^2/(N-M),$$

where N is the number of points, M is the number of parameters, ω is the angular frequency, $P_1 \ldots P_M$ are parameters. Parameter r_c is defined as

$$r_c^2 = \sum_{i=1}^{N} \frac{\left(Z_i^{'} - Z_{i_{calc}}^{'}\right)^2 + \left(Z_i^{"} - Z_{i_{calc}}^{"}\right)^2}{Z_i^{'2} + Z_{i_{calc}}^{'\ 2}},$$

where i corresponds to the measured values of impedance and i_{calc} is attributed to the calculated values.

Results and discussion

Structure and morphology of TiO_2/BDD electrode

Evolution of electrode surface morphology

The surface of composite electrodes was analysed using Scanning Electron Microscope (SEM) (see Fig. 2). It is noticeable that the morphology of titania nanotubes formed in the anodization process is typical for such structures. The obtained nanotubes have regular anatase crystalline structure, with the internal diameter and length equal to about 30 nm and 8 μm, respectively. The BDD layer deposited on the surface of titania NTs is semi-continuous and consists of nanocrystals ranging in size from 100 to 400 nm in dependence on the [B]/[C] ratio (Fig. 2a - c). According to the published literature, under ideal crystallizations conditions, i.e. high quality silicon substrate, the size of BDD nanocrystals decreases with increasing boron-doping level.[46] In order to demonstrate the effect of TiO_2 support on the performance of composite structure, in Fig. 2e we present the morphology of freshly anodized TiO_2 nanotube array for comparative purposes. Nevertheless, in the case of BDD deposited onto titania NTs, the correlation between the boron-level and the mean size of nanocrystals is not evident due to inhomogeneity of NTs substrate. We postulate that the surface of titania NTs causes disturbances during the pre-treatment step of nanodiamond seeding *via* agglomeration of seeding media. Furthermore, the

sharp edges of titania NTs can possibly serve as the initial sites of diamond crystallization. Despite the aforementioned effects, the significantly smaller grains of TiO_2/BDD-10k than those obtained for TiO_2/BDD-2k or TiO_2/BDD-5k electrodes can be noticed in Fig. 2a-c. Figure 2d shows the fragment of composite electrode with a partially removed surface layer. The unaffected, highly ordered structure of titania nanotubes can be observed under the BDD nanocrystalline layer, which proves that the nanotube structure had not been corrupted during MW PA CVD process.

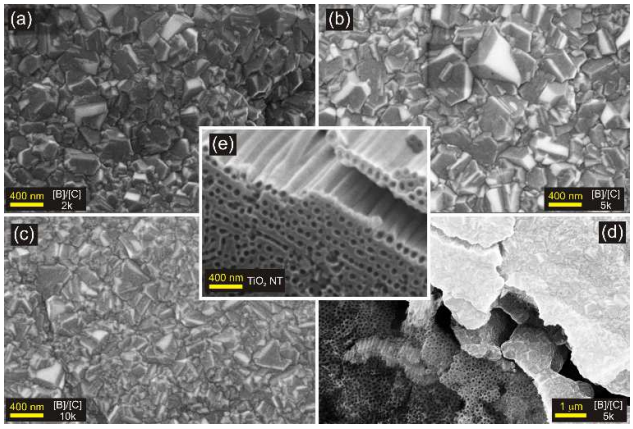

Fig. 2 SEM images of electrode surface recorded for samples with B/C ratio at: (a) – 2000 ppm, (b) – 5000 ppm, (c) – 10000 ppm, (e) - freshly anodized TiO_2 nanotube array. In Fig. (d) the diamond layer is partially removed from the surface and unaffected TiO_2 nanotube structure can be observed.

Investigation of electrode structure by Raman spectroscopy

The Raman analysis of titania nanotubes, prepared as a substrate for the BDD nanocrystalline layer, showed their pure anatase structure with the main Raman bands at 144, 394, 514 and 634 cm^{-1} (Fig. 3a). The spectra recorded for composite electrodes containing different concentrations of boron are presented in Figs. 3b and 3c (inset with enlarged detail). The lack of strong titania bands in the Raman spectra recorded for composite electrodes results from the strong absorption of Raman signal at the interface between titania nanotubes and the BDD layer.

The Raman spectra of BDD differ from standard diamond spectra. Besides the narrow sp^3 band at 1332 cm^{-1}, a relatively intense and wide sp^2 band located near 1500 – 1550 cm^{-1} and the narrow band characteristic for nanocrystalline diamond with a maximum at 1130 cm^{-1} can be observed. The wide bands in the 2800 – 3100 cm^{-1} region originate from the CH stretching vibrations.

Table 1 The peak position and full width at half maximum of the sp^3 line vs. various [B]/[C] ratio in plasma and substrate material.

Sample	sp^3 peak position [cm^{-1}]	FWHM [cm^{-1}]
Ti/BDD-5k	1318.6	29.6
TiO_2/BDD-10k	1312.7	26.8
TiO_2/BDD-5k	1310.2	22.1
TiO_2/BDD-2k	1330.1	17.1

Depending of the [B]/[C] ratio, additional bands with the maxima at 500 cm^{-1} and 1220 cm^{-1} can be observed. The origin of bands at 500 and 1220 cm^{-1} is not fully explained but they can be attributed to lattice disorder and intra-band optical transitions caused by the presence of boron[47–49]. The intensity of these two bands depends of the boron-doping level and is negligible for the sample with the [B]/[C] ratio at 2000 ppm level.

The shift of 1332 cm^{-1} diamond sp^3 band position and its width variation (see Table 1) originate from a quantum interface between the phonon and the continuum of electronic state in a degenerate semiconductor when the diamond film exhibits metallic conductivity[49–51]. As can be observed in Fig. 3c, in samples with the [B]/[C] ratio of 5000 and 10000 ppm this band has shifted to the lower wavenumbers and is noticeably broadened compared to the sample with the ratio at 2000 ppm level. Due to anisotropic structure of titania nanotubes/BDD composite material it's electrochemical properties will vary depending on the orientation i.e. parallel or perpendicular to nanotubes axes. In this paper the electrochemical properties of continuous electrode film are investigated and the composite material is considered as two-dimensional structure. The detailed description of the internal structure and its influence on electrochemical properties requires additional studies.

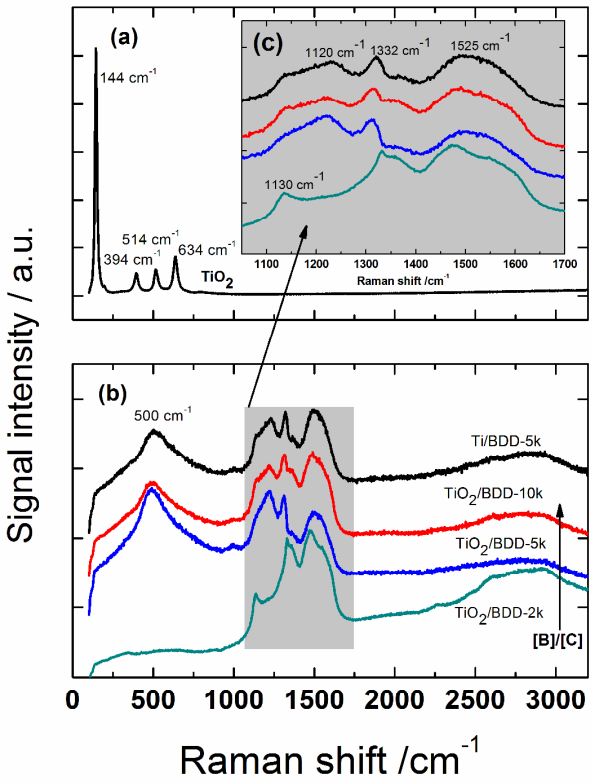

Fig. 3 Raman spectra of titania nanotubes (a) and BDD coated composite electrodes (b) with [B]/[C] ratio of 2000 ppm (1), 5000 ppm (2), 10000 ppm (3) and BDD with [B]/[C] = 5000 ppm deposited on Ti substrate; The inset (c) shows a zoom of the 1000-1700 cm^{-1} Raman spectra region recorded for composite electrodes.

Electrochemical studies of TiO_2/BDD electrode

Cyclic voltammetry (CV)

Cyclic voltammetry (*CV*) is regarded as a very useful and easy method for investigating electrochemical properties of the materials interface in contact with electrolyte. Fig. 4 shows the cyclic voltammetry curves of pure titania nanotubes, BDD layer and composite materials, i.e. TiO_2 coated with BDD with the [B]/[D] ratios of 2k, 5k and 10k prepared in the gas phase. For all tested materials, titanium plate served as a substrate. In comparison to the single films of TiO_2 nanotube arrays and BDD, BDD/TiO_2 materials exhibited clear capacitive character. The shape of *CV* curves recorded for composite electrodes is almost rectangular without redox peaks which indicates the presence of the double layer capacitance (C_{dl})[52]. Taking into account the anodic current density at plateau present at -0.2 V *vs*. Ag/AgCl/0.1M KCl and the relationship between C_{dl} and the potential sweep rate $C_{dl} = j/v$, the double layer capacitance was estimated. The specific capacitance of TiO_2/BDD layers equaled 2.10, 4.79, 7.46 mF cm^{-2} for the respective [B]/[C] ratios of 2k, 5k and 10k at a scan rate of 10 mV/s, whereas for the pure BDD film, the value of C_{dl} reached only 0.11 mF/cm^{-2}. In general, without taking into account layer thickness and electrochemical conditions used for electrode testing, the specific capacitance of boron-doped diamond deposited onto the titania nanotube layer was higher in comparison to self-doped TiO_2 (1.84 mF cm^{-2})[8], hydrogenated TiO_2 nanotubes (7.22 mF cm^{-2})[5], (3.24 mF cm^{-2})[9] and composite electrode materials such as BDD/carbon nanotubes[53] or BDD/carbon fibres[54] (1.94 mF cm^{-2}). However, when electrode layer thickness was considered, the volume capacitance for TiO_2/BDD-10 equals 8.9 F cm^{-3} that is significantly higher than obtained for hydrogenated nanotubes (5 F cm^{-3}) or BDD/carbon nanotubes structure (0.47 F cm^{-3}). Nevertheless, valuable comparison of electrochemical properties could be undertaken when all other electrode materials would be tested in the same chemical environment.

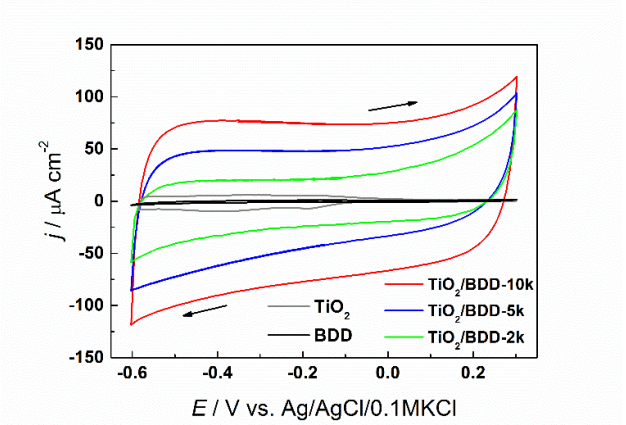

Fig. 4 Cyclic voltammetry curves registered for composite electrodes TiO_2/BDD with different [B]/[C] ratio and as reference for pure titania and BDD layer immersed in 0.1 M $NaNO_3$ (10 mV/s).

It is known that the double-layer charging current is strongly related to the real surface area of electrode material. Therefore, in the case of TiO_2/BDD system, an increase in the measured current obviously results from the presence of titania nanotubes that served as a substrate for BDD growth; the extended BDD surface has contact with an electrolyte as has been observed for other porous substrates.[55,56] A clear difference between the TiO_2/BDD layers obtained at various [B]/[C] ratios in the gas phase was also observed. According to previous studies in which the electrical and electrochemical properties of BDD layers with different [B]/[C] ratios were studied[57,58] an increase in boron concentration resulted in the higher conductivity of samples, and therefore in the enhanced capacitance current. It should be noted that the boron content could also affect the surface roughness, resulting in an additional increase in surface area. However, as illustrated by the SEM images, a significant difference between the analyzed composite materials has not been observed in this study. Thus, most likely, the changes in layer conductivity played a crucial role here.

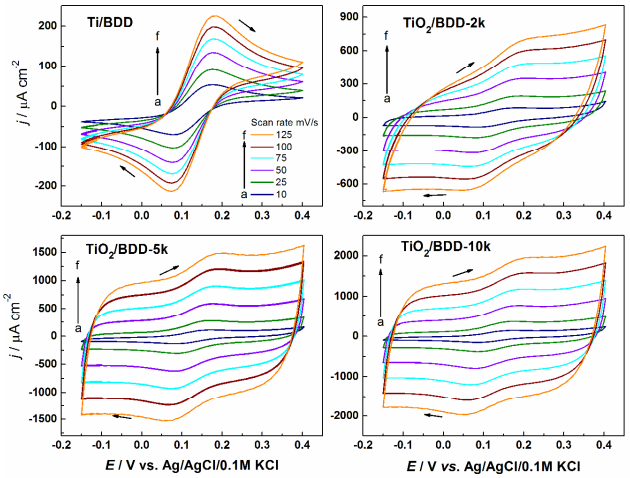

Fig. 5 Cyclic voltammetry curves of BDD and BDD/TiO_2 electrodes in 1 mM $K_3(FeCN)_6$/0.1M $NaNO_3$ with varies scan rates of a) 10, b) 25, c) 50, d) 75, e) 100, f) 125 mV/s.

The ferii/feroocyanide redox system is characterized by the inner-sphere electron transfer process with kinetics that is sensitive to surface properties, i.e. sp^2 bonded carbon or the density of electronic states near the formal potential. Cyclic voltammetry curves for the ferii/ferrocyanide redox couple exhibited the usual set of reduction and oxidation current peak for all the tested electrodes. Fig. 5 presents *CV* curves obtained for BDD and TiO_2/BDD electrodes immersed in 1 mM $K_3Fe(CN)_6$/0.1M $NaNO_3$ at different scan rates and with cathodic pre-treatment at -0.1 V *vs*. Ag/AgCl/0.1M KCl for 60 s that provides reversible response.[59] In general, an increase in sweeping rate promotes the growth of current peak intensity in cathodic and anodic reaction as well. As in the case of C*V* registered in 0.1M $NaNO_3$ alone, the current density for all TiO_2/BDD electrodes was higher than that observed in pure BDD film, which reflects the characteristic charging current. Additionally, the redox reaction rate increases with increasing boron-doping level due to the enhanced density of electronic states.[46,60] The degree of reversibility was the same for all testes samples independently of their [B]/[C] ratio and the type of substrate used for BDD growth (flat Ti or TiO_2 nanotubes). Similar reversibility could result from: a) the cathodic pre-treatment applied to all tested electrodes[59], and b) the presence of titania nanotube support providing the large surface area for BDD loading and causing higher boundary density. As in the case of electrode performance in 0.1 M $NaNO_3$, where the electrode was in contact with the ferii/ferocyanide redox system, the enhancement of recorded current could be related to

a decrease in the sp^3/sp^2 ratio and an increase in the electrical conductivity for higher boron concentrations.

Electrochemical Impedance Spectroscopy (EIS)

The electrochemical impedance spectroscopy (*EIS*) is regarded as a highly effective, non-destructive method to evaluate the electrochemical performance of electrode material[61]. In Fig. 6 the Nyquist plots of impedance spectra recorded and fitted for titania nanotubes decorated by BDD and, as a reference, for BDD deposited onto Ti substrate in contact with 1 mM $[Fe(CN)_6]^{3-/4-}$/1 M $NaNO_3$ are presented.

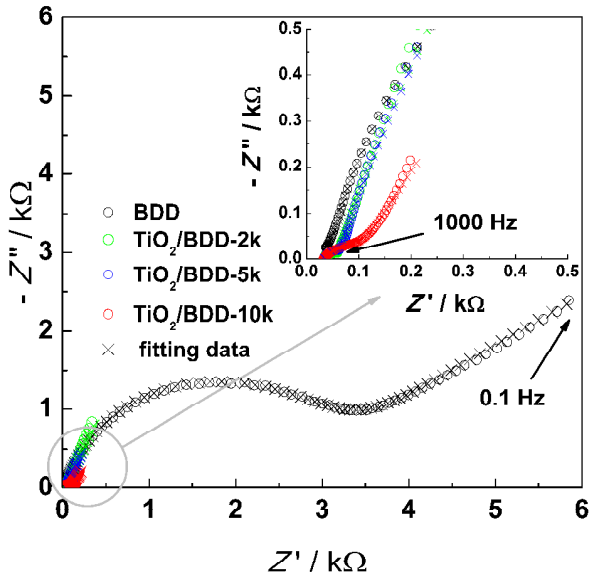

Fig. 6 Impedance spectra for TiO_2/BDD electrodes and BDD film in 1 mM $K_3Fe(CN)_6$ + 0.1 M $NaNO_3$ at E_f = + 0.13 V *vs.* Ag/AgCl/0.1M KCl.

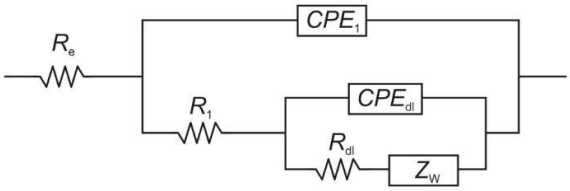

Scheme 1 Schematic depiction electrical equivalent circuit used for the fitting procedure for both BDD and composite electrodes.

The collected spectra were analysed using electric equivalent circuit (*EEQC*) with the elements in the model that reflects the physical electrochemistry of the system that is in contact with electrolyte. Proposed *EEQC* containing typical Randles arrangement given in Scheme 1 and is similar to circuit proposed by Wang *et al.*[62] The fitting procedure gives normalized fitting errors in optimal solution at the level of 10^{-5}. The ohmic resistance element in the high frequency regime represents electrolyte resistance; it was similar for all tested materials, i.e. ~ 34 Ω. The R_1 and CPE_1 elements are attributed to bulk resistance and space charge bulk capacitance of material. R_{ct} and CPE_{dl} that arises in the high frequency regime represents the charge transfer resistance and the double layer capacitance, respectively. The *W* element, called Warburg impedance, describes the mass transport impedance and is assigned to the diffusion of charged species from the bulk of electrolyte to the interface and through the interface layer. The constant phase elements could be treated as capacitance because the electrode surface is not exactly flat and infinitely large (see SEM microimages in Fig. 2).

The impedance of *CPE* is characterized by impedance $Z = Q^{-1}(i\omega)^{-n}$, where ω is angular frequency, Q is *CPE* parameter and n is exponential. The n values for *CPE* elements vary from 0.92 to 0.96. We consider that the elements CPE_1 and R_1, arising in the high frequency regime, are related to the electrode properties (*i.e.* porosity[63]) and are independent of the kinetics of Faradaic charge transfer.

Table 2 Values of double layers capacitance and charge transfer resistance calculated from the *EEQC* for composite materials and pure BDD layer.

Sample	Q_{dl} [$\mu\Omega^{-1}cm^{-2}s^n$]	R_{ct} [$k\Omega\ cm^2$]
Ti/BDD-5k	4.2	3037
TiO_2/BDD-2k	1280	1700
TiO_2/BDD-5k	2500	1200
TiO_2/BDD-10k	4460	220

The values of R_{ct} and CPE_{dl} collected in Table 2 are surface-dependent, with the pure BDD sample having the highest resistance and TiO_2/BDD-10k having the highest capacitance. This phenomenon could be reasonably explained by the best conductivity[64] of TiO_2/BDD-10k electrode from among all tested samples due to its highest boron content in the composite layer. A comparative analysis of Q_{dl} values calculated for all samples shows that the composite material with [B]/[C] ratio of 10000 has the double layer capacitance 800 times larger than the BDD layer alone. As it is known,[65] the electrochemically active surface area states as a significant feature in the low frequency region. Highly developed surface area allows more charge to pass by that lead to impedance reduction. Because we assumed Ti/BDD surface as rather smooth, the capacitance of 4.2 $\mu\Omega^{-1}cm^{-2}s^n$ corresponds to 1 cm^2 geometric surface area. Taking into account Q_{dl} values, the real, electroactive surface area could be determined as follows i.e. for TiO_2/BDD-10k: 4460/4.2 = 1062 cm^2. Therefore, active surface area of other TiO_2/BDD composite materials could be estimated as: 304 for TiO_2/BDD-2k and 595 cm^2 for TiO_2/BDD-5k. Furthermore, observed significant decrease in the charge transfer resistance values, could be also related to the boron content in the gas phase. As mentioned earlier, an increase in the boron content enhances conductivity and the charge transfer resistance. Because of that the highest reduction of surface resistance was achieved for TiO_2/BDD-10k electrode.

Conclusion

We proposed to enhance the electrochemical properties of anodized TiO_2 nanotube array by using the highly conductive boron-doped CVD diamond overlayer. All the composite TiO_2/BDD electrodes were characterized by the significantly higher current than both the BDD layer and pure titania nanotubes deposited directly onto Ti substrate.

The Raman spectra of the BDD layer on TiO_2 nanotubes differed from standard diamond spectra. Besides the narrow sp^3 band at 1332 cm^{-1}, a relatively intense and wide sp^2 band located near 1500 – 1550 cm^{-1} and the narrow band

characteristic for nanocrystalline diamond with a maximum at 1130 cm^{-1} were observed. The lack of strong titania bands was attributed to the low transparency of BDD layer encapsulating the nanotube arrays.

The novel composite electrode, consisting of TiO_2 nanotube arrays overgrown by boron-doped diamond (BDD), immersed in 0.1 M $NaNO_3$ can deliver specific capacitance of 2.10, 4.79, 7.46 mF cm^{-2} at a scan rate of 10 mV/s for the [B]/[C] ratio of 2, 5 and 10k, respectively. The substantial improvement of electrochemical performance, excellent rate capability and cycling stability can be attributed to the synergistic effect of TiO_2 treatment in CH_4:H_2 plasma and the high electrical conductivity of BDD overlayer.

The analysis of electrochemical impedance spectra, according to the electric equivalent circuit $R_e(CPE_1(R_1(CPE_{dl}(R_{dl}W))))$, allowed us to determine most of all charge transfer resistance and surface area based on the value of constant phase element. The electroactive surface area estimated on the basis of charge transfer capacitance value was significantly higher in comparison to the flat BDD layer. Based on *CV* and *EIS* analysis, it can be concluded that boron concentration is responsible for a decrease in charge transfer and bulk resistance, and a significant increase in the double layer capacitance. Furthermore, electrochemical tests showed that TiO_2/BDD composites can be regarded as promising electrode materials for supercapacitors.

The research shows, that the structure of presented here material is not a simple titania nanotubes/BDD interface but its internal structure is more complicated. The detailed study of the composite material internal structure, including cross-sectional SEM, Raman and XPS are currently under investigation and the results will be reported soon.

Acknowledgements

The authors gratefully acknowledge financial support from the Polish National Science Centre (NCN) under Grant No. 2011/03/D/ST7/03541 and No. 2012/07/D/ST5/02269. The DS funds of the Faculty of Electronics, Telecommunications and Informatics of the Gdansk University of Technology are also acknowledged.

Notes and references

[a] Centre for Plasma and Laser Engineering, The Szewalski Institute of Fluid-Flow Machinery, Polish Academy of Sciences, 14 Fiszera St., 80-231 Gdansk, Poland.
[b] Department of Metrology and Optoelectronics, Faculty of Electronics, Telecommunications and Informatics, Gdansk University of Technology, 11/12 G. Narutowicza St., 80-233 Gdansk, Poland.

1. G. Yu, L. Hu, M. Vosgueritchian, H. Wang, X. Xie, J. R. McDonough, X. Cui, Y. Cui, and Z. Bao, *Nano Lett.*, 2011, **11**, 2905–2911.
2. J. Bae, M. K. Song, Y. J. Park, J. M. Kim, M. Liu, and Z. L. Wang, *Angew. Chem. Int. Ed.*, 2011, **50**, 1683–1687.
3. P. Simon and Y. Gogotsi, *Nat Mater*, 2008, **7**, 845–854.
4. X. Lang, A. Hirata, T. Fujita, and M. Chen, *Nat Nano*, 2011, **6**, 232–236.
5. H. Wu, C. Xu, J. Xu, L. Lu, Z. Fan, X. Chen, Y. Song, and D. Li, *Nanotechnology*, 2013, **24**, 455401.
6. A. Burke, *Journal of Power Sources*, 2000, **91**, 37–50.
7. M. Salari, S. H. Aboutalebi, A. T. Chidembo, I. P. Nevirkovets, K. Konstantinov, and H. K. Liu, *Phys. Chem. Chem. Phys.*, 2012, **14**, 4770–4779.
8. H. Zhou and Y. Zhang, *J. Phys. Chem. C*, 2014, **118**, 5626–5636.
9. X. Lu, G. Wang, T. Zhai, M. Yu, J. Gan, Y. Tong, and Y. Li, *Nano Lett.*, 2012, **12**, 1690–1696.
10. S.-C. Li, Z. Zhang, D. Sheppard, B. D. Kay, J. M. White, Y. Du, I. Lyubinetsky, G. Henkelman, and Z. Dohnálek, *J. Am. Chem. Soc.*, 2008, **130**, 9080–9088.
11. Z. Wang, C. Yang, T. Lin, H. Yin, P. Chen, D. Wan, F. Xu, F. Huang, J. Lin, X. Xie, and M. Jiang, *Adv. Funct. Mater.*, 2013, **23**, 5444–5450.
12. T. Leshuk, R. Parviz, P. Everett, H. Krishnakumar, R. A. Varin, and F. Gu, *ACS Appl. Mater. Interfaces*, 2013, **5**, 1892–1895.
13. J. Xu, K. Wang, S.-Z. Zu, B.-H. Han, and Z. Wei, *ACS Nano*, 2010, **4**, 5019–5026.
14. Y.-Q. Dou, Y. Zhai, H. Liu, Y. Xia, B. Tu, D. Zhao, and X.-X. Liu, *Journal of Power Sources*, 2011, **196**, 1608–1614.
15. L. Shen, X. Zhang, H. Li, C. Yuan, and G. Cao, *J. Phys. Chem. Lett.*, 2011, **2**, 3096–3101.
16. D. Yuan, T. Zhou, S. Zhou, W. Zou, S. Mo, and N. Xia, *Electrochemistry Communications*, 2011, **13**, 242–246.
17. X. Xia, J. Tu, Y. Mai, X. Wang, C. Gu, and X. Zhao, *J. Mater. Chem.*, 2011, **21**, 9319–9325.
18. R. Menéndez, P. Alvarez, C. Botas, F. Nacimiento, R. Alcántara, J. L. Tirado, and G. F. Ortiz, *Journal of Power Sources*, 2014, **248**, 886–893.
19. D. Yu and L. Dai, *J. Phys. Chem. Lett.*, 2010, **1**, 467–470.
20. B. O. Boskovic, V. B. Golovko, M. Cantoro, B. Kleinsorge, A. T. H. Chuang, C. Ducati, S. Hofmann, J. Robertson, and B. F. G. Johnson, *Carbon*, 2005, **43**, 2643–2648.
21. P. W. May, *Science*, 2008, **319**, 1490 –1491.
22. R. S. Sussmann, *CVD diamond for electronic devices and sensors*, J. Wiley, Chichester, U.K., 2009.
23. Asmussen/Reinha and D. K. Reinhard, *Diamond Films Handbook*, CRC Press, 2002.
24. A. Kraft, *International Journal of Electrochemical Science*, 2007, **2**, 355–385.
25. H. Kato, J. Hees, R. Hoffmann, M. Wolfer, N. Yang, S. Yamasaki, and C. E. Nebel, *Electrochemistry Communications*, 2013, **33**, 88–91.
26. D.-W. Wang, F. Li, Z.-G. Chen, G. Q. Lu, and H.-M. Cheng, *Chem. Mater.*, 2008, **20**, 7195–7200.
27. A. S. Barnard, S. P. Russo, and I. K. Snook, *Nano Lett.*, 2003, **3**, 1323–1328.
28. O. Shenderova, D. Brenner, and R. S. Ruoff, *Nano Lett.*, 2003, **3**, 805–809.
29. N. Yang, H. Uetsuka, E. Osawa, and C. E. Nebel, *Angewandte Chemie International Edition*, 2008, **47**, 5183–5185.
30. B. J. M. Hausmann, M. Khan, Y. Zhang, T. M. Babinec, K. Martinick, M. McCutcheon, P. R. Hemmer, and M. Lončar, *Diamond and Related Materials*, 2010, **19**, 621–629.
31. M. Karlsson, P. Forsberg, and F. Nikolajeff, *Langmuir*, 2010, **26**, 889–893.
32. Y. Zou, P. W. May, S. M. C. Vieira, and N. A. Fox, *Journal of Applied Physics*, 2012, **112**, 044903.
33. C. Y. Cheng, M. Nakashima, and K. Teii, *Diamond and Related Materials*, 2012, **27–28**, 40–44.
34. C. Terashima, K. Arihara, S. Okazaki, T. Shichi, D. A. Tryk, T. Shirafuji, N. Saito, O. Takai, and A. Fujishima, *ACS Appl. Mater. Interfaces*, 2011, **3**, 177–182.

35. A. T. H. Chuang, B. O. Boskovic, and J. Robertson, *Diamond and Related Materials*, 2006, **15**, 1103–1106.
36. N. A. Braga, C. A. A. Cairo, M. R. Baldan, V. J. Trava-Airoldi, and N. G. Ferreira, *Diamond and Related Materials*, 2011, **20**, 31–35.
37. H. Masuda, M. Watanabe, K. Yasui, D. Tryk, T. Rao, and A. Fujishima, *Adv. Mater.*, 2000, **12**, 444–447.
38. D. A. H. Hanaor and C. C. Sorrell, *J Mater Sci*, 2011, **46**, 855–874.
39. R. Bogdanowicz, M. Gnyba, P. Wroczyński, and B. B. Kosmowski, *Journal Of Optoelectronics And Advanced Materials*, 2010, **12**, 1660 – 1665.
40. R. Bogdanowicz, *Acta Physica Polonica A*, 2008, **114**, A33–A38.
41. K. E. Bennet, K. H. Lee, J. N. Kruchowski, S.-Y. Chang, M. P. Marsh, A. A. Van Orsow, A. Paez, and F. S. Manciu, *Materials*, 2013, **6**, 5726–5741.
42. S. C. B. Oliveira and A. M. Oliveira-Brett, *Electrochimica Acta*, 2010, **55**, 4599–4605.
43. E. Brillas and C. A. M. Huitle, Eds., *Synthetic Diamond Films: Preparation, Electrochemistry, Characterization and Applications*, Wiley, Hoboken, N.J, 1 edition., 2011.
44. A. L. Pomerantsev, *Progress in Chemometrics Research*, Nova Biomedical, New York, 1 edition., 2005.
45. L. Lu, B. H. Brown, D. C. Barber, and A. D. Leathard, *Physiol. Meas.*, 1995, **16**, A39.
46. R. Bogdanowicz, A. Fabiańska, L. Golunski, M. Sobaszek, M. Gnyba, J. Ryl, K. Darowicki, T. Ossowski, S. D. Janssens, K. Haenen, and E. M. Siedlecka, *Diamond and Related Materials*, 2013, **39**, 82–88.
47. E. Gheeraert, P. Gonon, A. Deneuville, L. Abello, and G. Lucazeau, *Diamond and Related Materials*, 1993, **2**, 742–745.
48. P. Gonon, E. Gheeraert, A. Deneuville, F. Fontaine, L. Abello, and G. Lucazeau, *Journal of Applied Physics*, 1995, **78**, 7059–7062.
49. K. Ushizawa, K. Watanabe, T. Ando, I. Sakaguchi, M. Nishitani-Gamo, Y. Sato, and H. Kanda, *Diamond and Related Materials*, 1998, **7**, 1719–1722.
50. M. Mermoux, F. Jomard, C. Tavarès, F. Omnès, and E. Bustarret, *Diamond and Related Materials*, 2006, **15**, 572–576.
51. F. Pruvost, E. Bustarret, and A. Deneuville, *Diamond and Related Materials*, 2000, **9**, 295–299.
52. H. Wu, D. Li, X. Zhu, C. Yang, D. Liu, X. Chen, Y. Song, and L. Lu, *Electrochimica Acta*, 2014, **116**, 129–136.
53. H. Zanin, P. W. May, D. J. Fermin, D. Plana, S. M. C. Vieira, W. I. Milne, and E. J. Corat, *ACS Appl. Mater. Interfaces*, 2014, **6**, 990–995.
54. E. C. Almeida, M. R. Baldan, J. M. Rosolen, and N. G. Ferreira, *Diamond and Related Materials*, 2008, **17**, 1529–1533.
55. A. V. Diniz, N. G. Ferreira, E. J. Corat, and V. J. Trava-Airoldi, *Materials Research*, 2003, **6**, 57–61.
56. N. G. Ferreira, A. F. Azevedo, A. F. Beloto, M. Amaral, F. A. Almeida, F. J. Oliveira, and R. F. Silva, *Diamond and Related Materials*, 2005, **14**, 441–445.
57. N. R. Wilson, S. L. Clewes, M. E. Newton, P. R. Unwin, and J. V. Macpherson, *J. Phys. Chem. B*, 2006, **110**, 5639–5646.
58. G. R. Salazar-Banda, K. I. B. Eguiluz, A. E. de Carvalho, and L. A. Avaca, *Journal of the Brazilian Chemical Society*, 2013, **24**, 1206–1211.
59. S. C. B. Oliveira and A. M. Oliveira-Brett, *Electrochimica Acta*, 2010, **55**, 4599–4605.
60. Z. Yu, J. Wang, Q. Wei, L. Meng, S. Hao, and F. Long, *Transactions of Nonferrous Metals Society of China*, 2013, **23**, 1334–1341.
61. A. Lasia, in *Modern Aspects of Electrochemistry*, eds. B. E. Conway, J. O. Bockris, and R. E. White, Springer US, 2002, pp. 143–248.
62. D. Wang, Q. Ye, B. Yu, and F. Zhou, *Journal of Materials Chemistry*, 2010, **20**, 6910.
63. C. Hitz and A. Lasia, *Journal of Electroanalytical Chemistry*, 2001, **500**, 213–222.
64. H. Pan, J. Li, and Y. Feng, *Nanoscale Res Lett*, 2010, **5**, 654–668.
65. R. Ahmed and K. Reifsnider, *International Journal of Electrochemical Science*, 2011, **6**, 1159 – 1174.

